Kovove Mater. 55 2017 295–302
DOI: 10.4149/km_2017_4_295

Impression creep properties of hypoeutectic Mg-xSi alloys

M. Badri, S. M. Miresmaeili*, B. Nami

Shahid Rajaee Teacher Training University, Lavizan, 16788-15811 Tehran, Iran

Received 19 April 2016, received in revised form 12 October 2016, accepted 13 October 2016

Abstract

Impression creep behavior of as-cast Mg-xSi alloys (x = 0.5, 0.8, 1.2 wt.%) was studied under shear modulus-normalized stress values ranging from 0.009 to 0.016 at temperatures between 398 and 491 K. The results show that creep properties of these alloys are improved with increasing Si content under all the applied loads and temperatures, and Mg-1.2Si alloy has minimum creep rate and thus maximum creep resistance. It is attributed to the higher volume fraction of Mg_2Si, which can reduce grain boundary sliding during the creep test. Stress exponent of all the alloys is between 4.06 and 7.09 in the temperature range of 398 to 447 K. It is changed from the range of 3.96–4.89 to 8.62–12.62 under high-stress values at temperatures between 476 and 491 K. Creep activation energy under shear modulus-normalized stress of 0.010 and 0.012 is close to that of dislocation pipe diffusion of Mg. Under higher stress values at the high temperatures the creep activation energy is equal to that of Mg lattice diffusion. According to the obtained stress exponent values and creep activation energies, pipe-diffusion climb controlled dislocation creep is the dominant mechanism at temperatures between 398 and 447 K, which changes to power-law breakdown (PLB) under high-stress values at 476 and 491 K.

K e y w o r d s: Mg-Si alloys, impression creep, creep mechanism, microstructure

1. Introduction

Magnesium alloys are being extensively used in structural applications and aerospace industries due to their comparatively low density and high damping capacity compared with other structural metals [1]. However, these alloys, such as Mg-Al, show poor creep resistance at the temperature of above 120 °C [2]. Some Mg-Al alloys showing improved mechanical properties at elevated temperature are available; they are alloyed with elements Ca, RE, Sr and Si [3–6]. The enhanced creep properties of these alloys have been ascribed to both the formation of high melting point intermetallic compounds such as Al_2Ca, $Al_{11}RE_3$, Al_4Sr and Mg_2Si and decreasing of soft $Mg_{17}Al_{12}$ phase [3–6]. Moreover, the costly Mg alloys containing Zr, Ag, Y, Th, and rare earths have been developed to obtain the alloys with higher creep properties in comparing with Mg-Al alloys [7].

In developing a low-cost, high creep resistant Mg-based alloy in more conventional applications, the Mg-Si binary system shows an exceptional potential as a piston material because of formation of a considerable amount of Mg_2Si phase in the microstructure of these alloys [7]. It has been shown that Mg_2Si phase is formed in the microstructure of Si-containing magnesium alloys with two polygonal and Chinese script morphologies [8–9]. Mg_2Si phase exhibits special characteristic properties including the high melting point (1085 °C), high hardness (460 HV), low density (1.9 g cm^{-3}), and low thermal expansion coefficient (7.5×10^6 K^{-1}) [7]. Mg_2Si phase exists mainly in the interdendritic regions, hinders the grain boundary sliding at high temperature because of its above-mentioned properties [8].

Most of the researches carried out on the Mg-Si binary alloys, have focused on the hypereutectic alloys with 2 and 4 wt.% Si contents [7, 9]. Considering the binary phase diagram of Mg-Si alloys [7], these alloys have a high melting temperature, about 800 °C. Also, the time needed for dissolution of Si in Mg melt is too long. In such a case, protection of the melt against the oxidation is very difficult [10]. Moreover, in spite of the enhanced creep properties of hypereutectic Mg-Si al-

*Corresponding author: tel./fax: +98 21 22970052; e-mail address: s.m.miresmaeili@srttu.edu

Table 1. Chemical composition (wt.%) of the alloys

Alloy	Si	Mg
Mg-0.5Si	0.49	Bal.
Mg-0.8Si	0.76	Bal.
Mg-1.2Si	1.23	Bal.

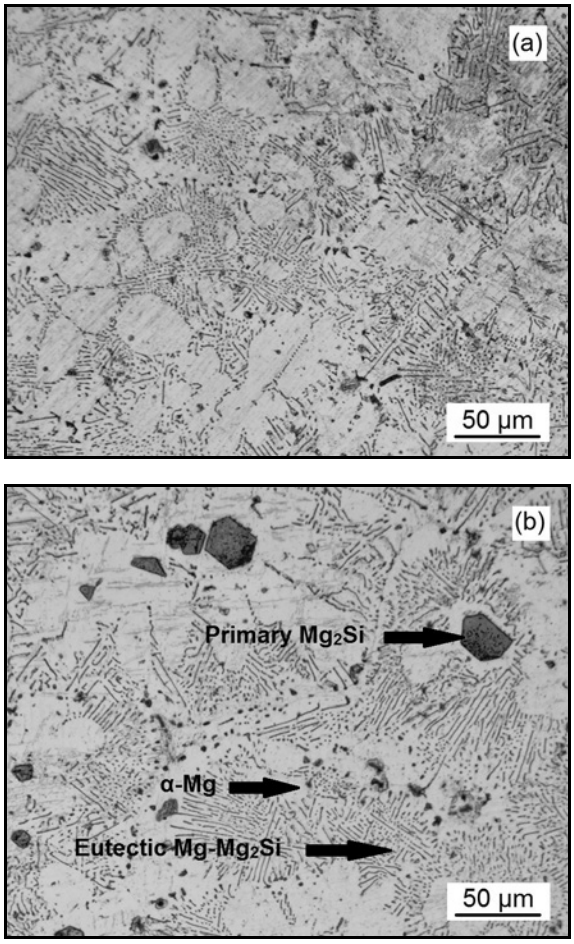

Fig. 1. The microstructure of the as-cast alloys, (a) Mg-0.8Si and (b) Mg-1.2Si.

loys due to the high amount of large, hard and brittle Mg_2Si phases, these compounds can deteriorate the alloys' room temperature mechanical properties [7, 9]. In this regard, the study on the microstructure and high-temperature mechanical properties of hypoeutectic Mg-Si alloys which have lower melting temperature and better room temperature mechanical properties than those of the hypereutectic alloys may be worth of note. Creep properties are one of the essential characteristics for utilizing of the alloys which are exposed at high service temperatures. The creep properties can be obtained either by conventional tensile creep test or by impression creep test. Impression creep technique

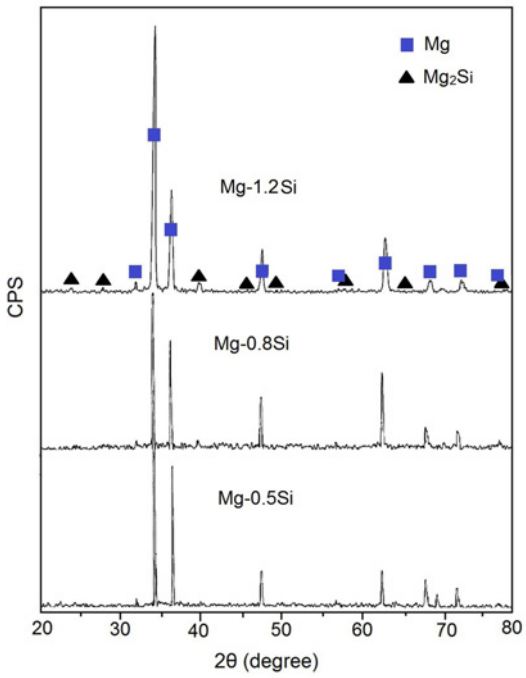

Fig. 2. XRD pattern of the Mg-xSi alloys.

developed by Chu and Li [11] is a modified method of indentation creep test. This technique has frequently been used to investigate the creep properties of magnesium alloys such as AZ91 [12], AM60 [13], MRI53 [14], Mg-5Sn [15], etc. However, no work has been carried out so far on the impression creep properties of Mg-Si alloys. Thus the aim of current study is to investigate the impression creep properties of three hypoeutectic Mg-Si alloys.

2. Experimental procedure

Commercial pure Mg ingot (99.9 % purity) and Si (99 % purity) were used to prepare Mg-xSi (x = 0.5, 0.8, and 1.2) alloys. The Mg ingot was melted at 760 °C in a graphite crucible under a protective atmosphere of mixed CO_2 and SF_6 gaseous in an electric resistant furnace. Silicon was preheated at 200 °C before adding to the melt. The melt alloys were then mechanically stirred and held for 30 min at 760 °C for complete dissolution of silicon. Finally, the melts were cast into a rectangular permanent mold with a dimension of 300 × 120 × 10 mm^3 preheated to 150 °C. The chemical composition of the alloys is listed in Table 1.

Slices with a dimension of 12 × 10 × 8 mm^3 were cut from the cast samples using a wire cut machine for impression creep testing. Microstructural investigation was carried out by an optical microscope and MIRA-TESCAN scanning electron microscope (SEM) equipped with an EDS analyzer. The alloys samples

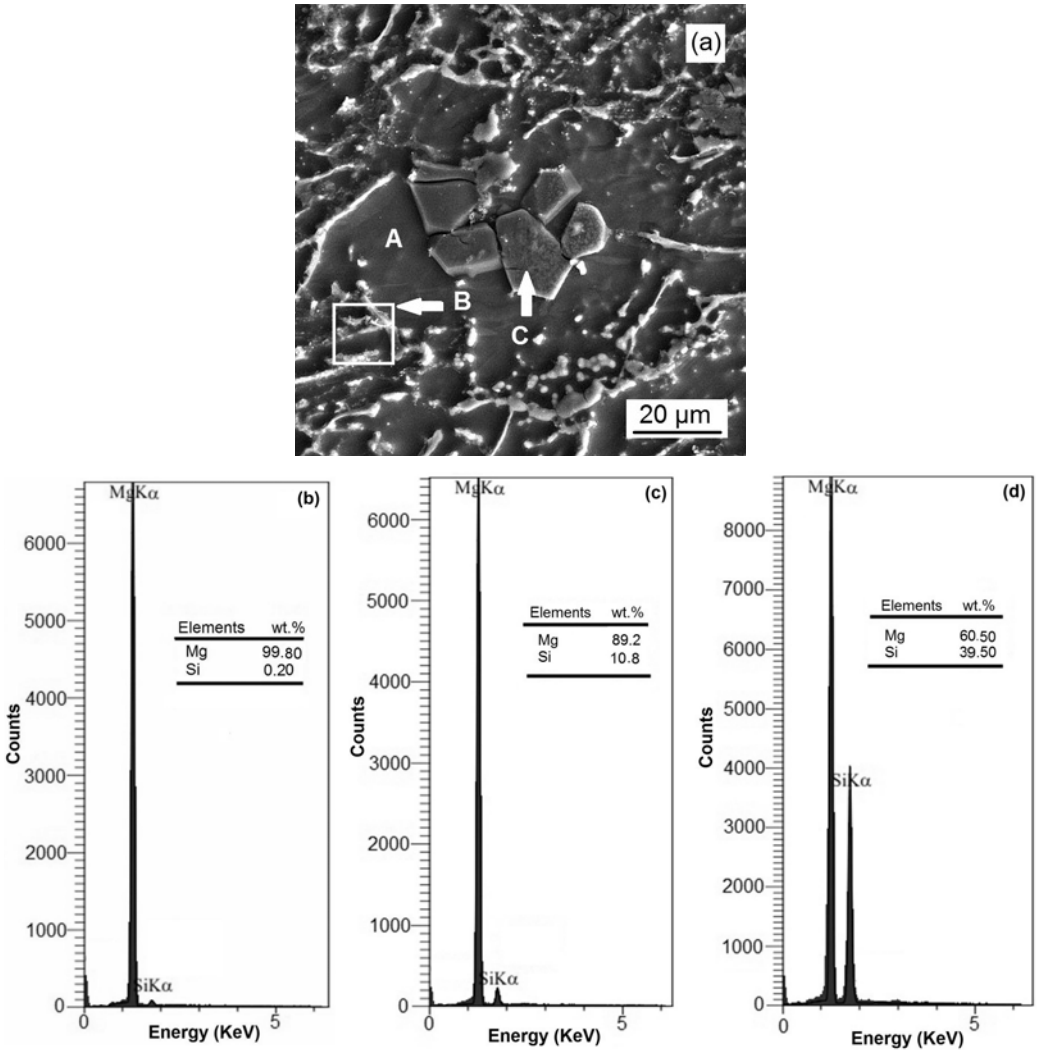

Fig. 3. SEM micrographs of Mg-1.2Si alloy; (a) SE image, (b) EDS spectrum of matrix phase, (c) EDS analysis obtained from the rectangular area, (d) EDS analysis of the polygonal phase.

were prepared by standard grinding-polishing methods and etched by 2 % nital solution (2 ml HNO_3 and 98 ml ethylic alcohol). Phase identification was performed by X-ray diffraction (XRD) method. Creep test was carried out using impression creep technique at the temperatures ranging from 398 to 491 K under shear modulus-normalized stresses (σ/G) between 0.009 and 0.016 for 5000 s. Detail of the impression creep test has been published elsewhere [5].

3. Results and discussion

3.1. Microstructure

Figure 1 shows the optical microscopy images of the as-cast Mg-0.8Si and Mg-1.2Si hypoeutectic magnesium alloys. The microstructure of Mg-0.8Si consists of primary α-Mg dendrites and a eutectic phase consists of α-Mg + β-Mg_2Si phases. As can be seen, the main microstructure constituent of the Mg-1.2Si alloy is similar to that of the Mg-0.8Si alloy. However, a new primary polygonal β-Mg_2Si phase is also observed in the alloy's microstructure. According to the Mg-Si binary equilibrium phase diagram [7], microstructure of hypo-eutectic Mg-Si alloys with silicon content less than 1.34 wt.%, consists of primary α-Mg and the eutectic phases. In this regard the presence of the primary β-Mg_2Si phase in the microstructure of the Mg--1.2Si alloy can be attributed to the non-equilibrium solidification process resulted from the high cooling rate solidification in the metallic mold used in the present research.

Figure 2 shows XRD pattern of the Mg-xSi alloys, confirming that the microstructure of these alloys consists of α-Mg and Mg_2Si phases, which has frequently been reported in the literature [7–9].

SEM micrograph of Mg-1.2Si alloy accompanied with EDS analysis obtained from the different phases in the microstructure is shown in Fig. 3. As seen in

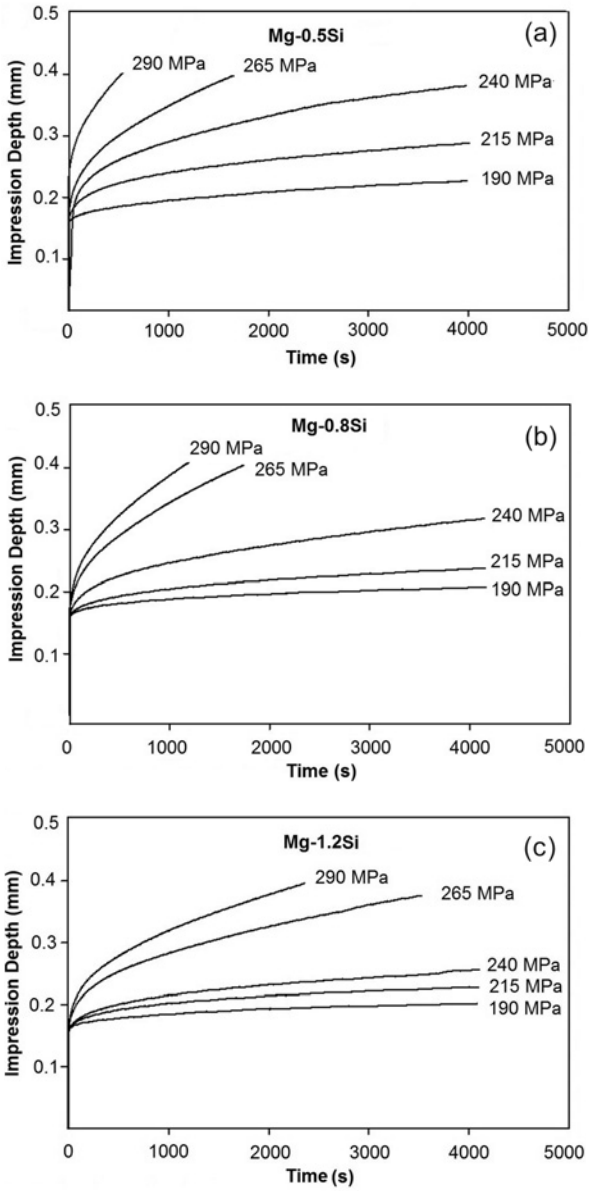

Fig. 4. Plots of variation of impression depth vs. time at 423 K for (a) Mg-0.5Si, (b) Mg-0.8Si, (c) Mg-1.2Si alloys.

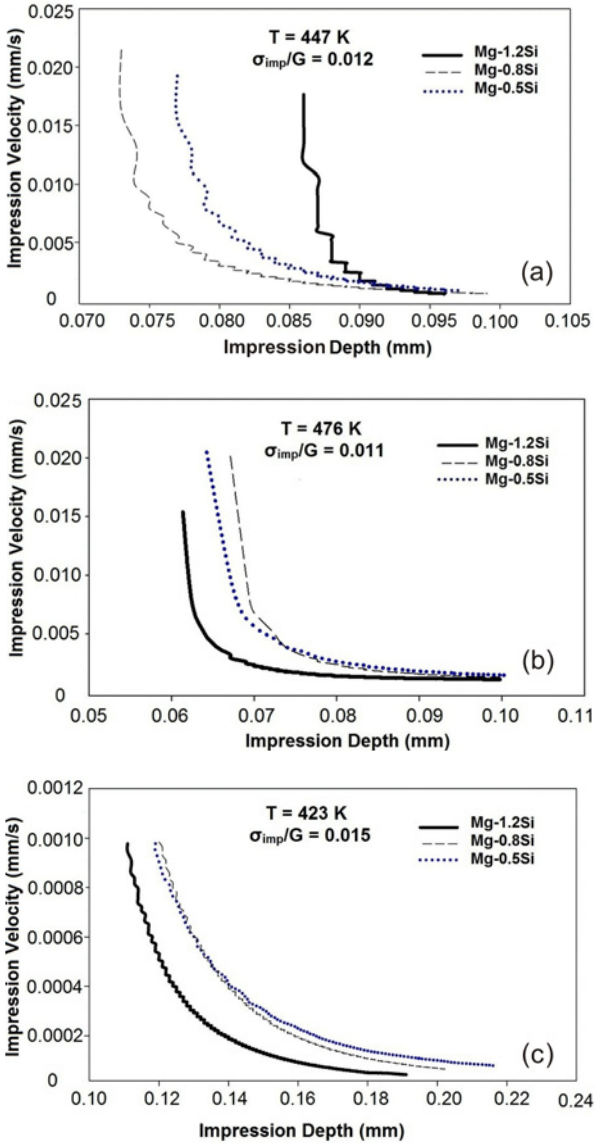

Fig. 5. Variation of minimum impression velocities with impression depth (a) $T = 423$ K, $\sigma_{\mathrm{imp}}/G = 0.015$; (b) $T = 447$ K, $\sigma_{\mathrm{imp}}/G = 0.012$; and (c) $T = 476$ K, $\sigma_{\mathrm{imp}}/G = 0.011$.

Fig. 3b, about 0.2 wt.% Si dissolved in the α-Mg matrix phase. The results of EDS microanalysis in Fig. 3c (rectangular in Fig. 3a), imply that the interdendritic phase is the eutectic mixture of α-Mg + Mg_2Si. Also, the EDS microanalysis obtained from the polygonal particles in Fig. 3a reveals that this phase can be the primary Mg_2Si phase.

3.2. Impression creep testing

Figures 4a–c typically show creep curves of the alloys tested at 423 K under different stress values. An instantaneous indentation is observed at the beginning of the test as shown in Fig. 4. This is the sum of primary elastic and plastic deformation resulted from the applied load. Although the primary instantaneous strain is increased with applied stress, its values were considered equal in drawing the creep curve for accurate comparing the impression depth resulted from creep deformation. Each of these impression curves shows a short primary stage of creep. They all demonstrate an approximately long steady-state region, in which the impression depth linearly increases with time. In fact, the creep rates remain constant over the testing time during the steady-state stage. Although the primary stage of creep is dominant during the creep test at high-stress values in Figs. 4a,b, i.e. 265 and 290 MPa, steady state creep is observed at the final stage of the creep test.

Comparison of these curves reveals that the creep

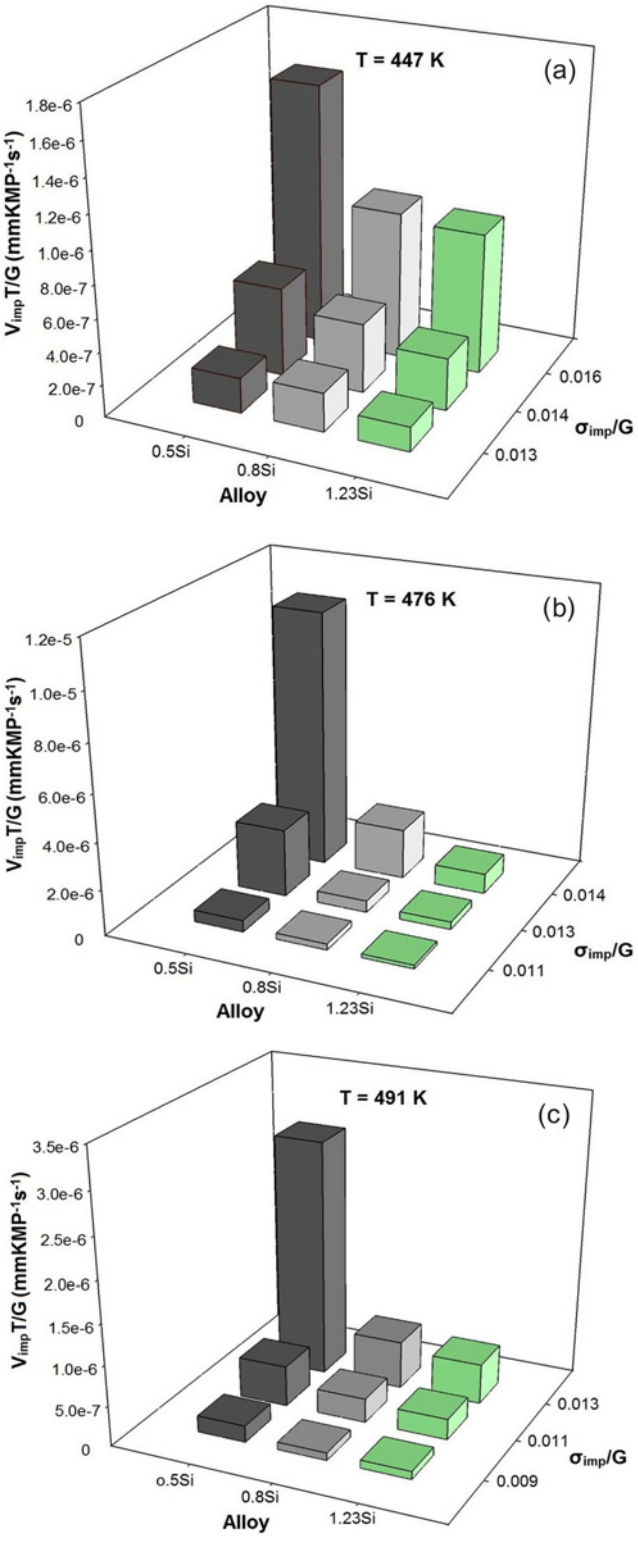

Fig. 6. Comparison of minimum creep rates obtained at different normalized stresses at (a) 447 K, (b) 476 K, (c) 491 K.

properties of Mg-xSi alloys have significantly improved by increasing Si amount.

To ensure that the steady-state creep regime is achieved in all of the specimens, impression velocity ($v_{\mathrm{imp}} = \mathrm{d}h/\mathrm{d}t$) is plotted against impression depth (h) on a semi-logarithmic scale at different temperatures under different shear modulus normalized stress values, as presented in Figs. 5a–c. Shear modulus of these alloys was obtained from the following equation [16]:

$$G\ (\mathrm{MPa}) = 19,200 - 8.6T\ (\mathrm{K}). \tag{1}$$

As seen, the penetration velocity of the indenter has decreased with time and reached to minimum values, indicating the dominance of steady-state creep stage. It is apparent that the creep rate has decreased with Si. Creep resistance of these alloys is also compared in Fig. 6 by plotting normalized steady-state impression velocity versus normalized punching stress at 3 different testing temperatures.

It can be observed that impression velocity has decreased with increasing Si content in all the testing conditions, implying the alloys' creep resistance improvement. However, this improvement is more considerable at the higher temperatures. Superior creep resistance of Mg-1.2Si alloy can be attributed to the higher volume fraction of Mg_2Si phase. According to the literature [5], intermetallic compounds can improve the strength of grain boundaries either by hindering dislocations annihilation, restricting their slipping inside the grains during the dislocation creep. Also, the creep properties can be enhanced by inhibiting the grain boundary migration or grain boundary sliding during diffusional and dislocation creep [17]. So, the main reason for enhancing the creep properties with increasing Si content may be explained by determining the dominant creep mechanism. This mechanism can be obtained by calculating both stress exponent (n) and creep activation energies (Q_{c}) in the following well-known equation relating the steady-state creep rate of a metallic material with the applied stress [18]:

$$\dot{\varepsilon} = A\left(\frac{b}{d}\right)^{p}\left(\frac{GbD_0}{kT}\right)\left(\frac{\sigma}{G}\right)^{n}\exp\left(-\frac{Q_{\mathrm{c}}}{RT}\right), \tag{2}$$

where $\dot{\varepsilon}$ is the minimum creep rate, A is material constant, b is Burgers vector, d is grain size, p is grain size power, G is shear modulus, D_0 is frequency constant, k is Boltzmann's constant, T is absolute temperature, σ is stress, and R is the gaseous universal constant.

This equation is suitable for conventional tensile creep. Therefore, the equivalent uniaxial creep strain rate ($\dot{\varepsilon}$) and stress (σ) can be obtained from impression velocity (V_{imp}) and impression stress (σ_{imp}) using the following semi-empirical relations [19]:

$$V_{\mathrm{imp}} = \frac{\mathrm{d}h}{\mathrm{d}t}, \tag{3}$$

$$\dot{\varepsilon} = \frac{V_{\mathrm{imp}}}{C_2\varphi}, \tag{4}$$

$$\sigma_{\mathrm{imp}} = \frac{4F}{\pi\varphi^2}, \tag{5}$$

$$\sigma = \frac{\sigma_{\mathrm{imp}}}{C_1}, \tag{6}$$

where h is indentation depth, t is time, φ is punch diameter, F is the applied load, and C_1 and C_2 are constants. The appropriate equation for the impression creep can be obtained by substituting Eqs. (3) to (6) in Eq. (2) as the following equation [18]:

$$\left(\frac{V_{\mathrm{imp}}T}{G}\right) = A\left(\frac{\varphi C_2}{C_1^n}\right)\left(\frac{b}{d}\right)^p\left(\frac{bD_0}{K}\right)\left(\frac{\sigma_{\mathrm{imp}}}{G}\right)^n \exp\left(-\frac{Q_{\mathrm{c}}}{RT}\right). \tag{7}$$

The stress exponent and creep activation energy can be obtained from the plot of $\ln(V_{\mathrm{imp}}T/G)$ versus $\ln(\sigma_{\mathrm{imp}}/G)$ at constant T and the plot of $\ln(V_{\mathrm{imp}}T/G)$ versus $1/T$ at constant σ_{imp}/G, respectively.

Figure 7 demonstrates the variation of $\ln(V_{\mathrm{imp}}T/G)$ versus $\ln(\sigma_{\mathrm{imp}}/G)$ for three alloys. As seen, the stress exponent varies between 4 and 7 at the temperature range of 398 to 447 K under all the applied stress values. According to Fig. 7, two distinct regimes with different slopes can be observed at the higher temperatures. Although the stress exponent values under lower stresses are similar to those shown at the lower temperatures, they are between 8 and 12 under higher stress levels.

Figure 8 shows the variation of $\ln(V_{\mathrm{imp}}T/G)$ versus $1/T$ at constant σ_{imp}/G. It is obvious that under the shear modulus-normalized stresses of 0.010 and 0.012 and at all the creep test temperatures, the activation energies are in the range of 70 to 88 kJ mol^{-1}. It can be seen that the creep activation energies of the specimens tested under the normalized stress values of more than 0.012 vary with the testing temperature. Although their values ($67 < Q < 84$ kJ mol^{-1}) at the temperatures of less than 447 K are similar to those obtained for the lower stress values, they increase at high temperatures. The obtained activation energies under low-stress values are close to that of Mg pipe diffusion, i.e. 92 kJ mol^{-1} [18]. Increasing activation energy at higher temperatures and under higher stress values to about 134 kJ mol^{-1} reveals that the diffusion during creep of the alloys occurs by Mg lattice diffusion.

Comparison of the obtained stress exponents and activation energies with those reported in the literature [18] reveals that pipe diffusion-climb controlled dislocation creep is the dominant mechanism during creep conditions in which the stress exponents are between 4 and 7. The transition of stress exponent from $n = 4$–7 to $n \geq 7$ observed at high-stress levels can be ascribed to power law breakdown (PLB) which frequently occurs in many metallic alloys at high-stress

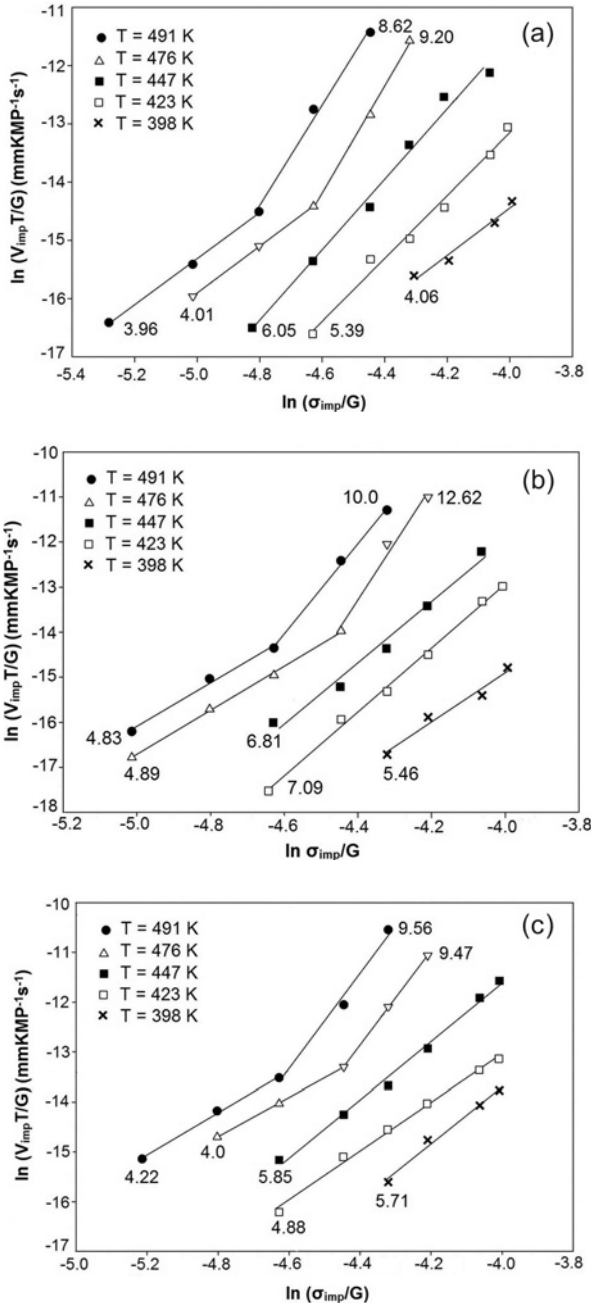

Fig. 7. Variation of $\ln(V_{\mathrm{imp}}T/G)$ vs. $\ln(\sigma_{\mathrm{imp}}/G)$ at constant T for calculating the stress exponent, (a) Mg-0.5Si, (b) Mg-0.8Si, and (c) Mg-1.2Si alloys.

values [18]. The stress exponent slightly higher than 8, however, may be relevant to the higher volume fraction of Mg_2Si in the alloys' microstructure.

Considering the obtained creep mechanism, it is possible to discuss how increasing Si content improves creep strength of these alloys. According to the literature, during climb controlled dislocation creep, high-temperature mechanical properties can be improved by decreasing of stacking fault energy, the forma-

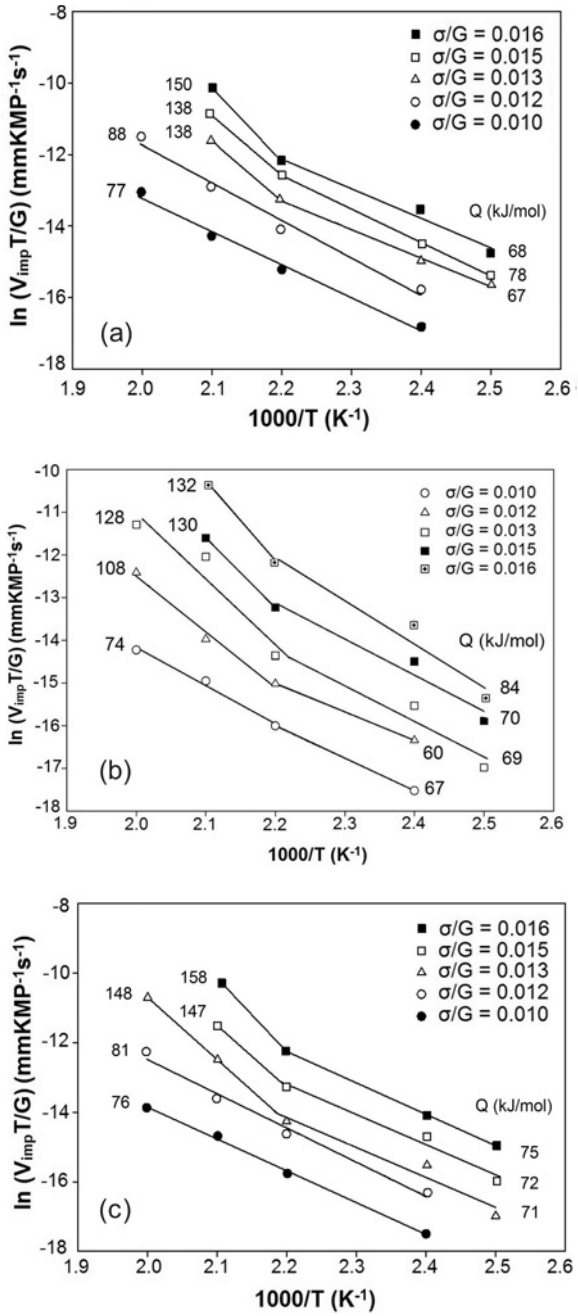

Fig. 8. Variation of $\ln(V_{\text{imp}}T/G)$ vs. $1/T$ at constant σ_{imp}/G to determine Q-values for: (a) Mg-0.5Si, (b) Mg--0.8Si, and (c) Mg-1.2Si alloys.

tion of particles with high thermal stability inside the grains, and forming intermetallic compounds in grain boundaries [20–23]. When the stacking fault energy is reduced, many dislocations are easily dissociated to partial dislocations with a wide stacking fault band. Climbing of partial dislocation is impossible separately, and it needs to be combined with each other before the climbing process. The stress needed for combining partial dislocation will increase with decreasing stacking fault energy. Intermetallic particles can act as barriers against the dislocations slipping inside the grains. They also can improve creep properties by hindering grain boundary sliding or preventing dislocation annihilation [20–23].

Wang et al. [24] showed that stacking fault energy of Mg decreases from 99.3 to 50.5 mJ m^{-2} with doping 0.69 % Si. According to EDS analysis in Fig. 3b, Si dissolves about 0.2 wt.% in α(Mg) matrix phase. Thus the reduced stacking fault energy due to the dissolved Si is one of the reasons which improve the creep properties of the alloys.

Also, the presence of the hard and thermally stable Mg_2Si particles as explained in the literature, in the grain boundary area can pin and prevent both grain boundary sliding and migration during high-temperature deformation. As shown in Fig. 1, the amount of Mg_2Si particles increased with Si content, leading to the better creep improvement with rising the Si amount.

4. Conclusions

Creep properties of Mg-xSi (x = 0.5, 0.8, and 1.2 wt.%) hypoeutectic alloys were investigated at 398 to 491 K under shear modulus normalized stress ranging from 0.009 to 0.016 using impression creep technique. The following results were obtained:

– The microstructure of the alloys is composed of α(Mg) matrix phase, eutectic Mg_2Si phase. A considerable amount of primary Mg_2Si phase was also formed in non-equilibrium solidified hypoeutectic Mg--1.2Si alloy. About 0.2 wt.% Si also dissolved in the α(Mg) matrix phase.

– The creep properties of the alloys improve with increasing Si content, which could be ascribed to the high volume fraction of Mg_2Si which hinders the grain boundary sliding during the creep process. Reducing stacking fault energy resulted by the dissolved Si could also be another reason for enhancing creep properties of the alloys.

– Depending on the stress values and temperatures, different values were obtained for stress exponent. The stress exponent values were between 4 and 7 at the temperatures less than 447 K under all the applied stress. Its values increased with stress to the values ranging from 8 to 12 at higher temperatures.

– A similar trend was observed for the creep activation energy. Under the shear modulus-normalized stresses of 0.010 and 0.012 and at all the testing temperatures, the activation energies were in the range of 70 to 88 kJ mol^{-1}. Creep activation energies of the specimens tested under the normalized stress values of more than 0.012 varied with the testing temperature. The activation energies values were between 67 and 84 kJ mol^{-1} at the temperatures less than 447 K,

whereas the values were increased with stress to the range of 128–158 (kJ mol^{-1}) at higher temperatures.

– Considering the obtained stress exponents and activation energies, pipe diffusion-dislocation climb controlled creep is the dominant mechanism at the temperature lower than 447 K. The dominant creep mechanism at higher temperatures depends on the stress level. Although pipe diffusion-dislocation climb controlled creep is the dominant mechanism under the low-stress regime, the creep rate is controlled by power law breakdown (PLB) mechanism under higher stress levels.

References

[1] Zhang, E., Wei, X., Yang, L., Xu, J., Song, Ch.: Mater. Sci. Eng. A, *527*, 2010, p. 3195. doi:10.1016/j.msea.2010.01.074

[2] Liao, L., Zhang, X., Wang, H.: Mater. Lett., *59*, 2005, p. 2702. doi:10.1016/j.matlet.2005.03.055

[3] Yong, H., Li, R.: China Foundry, *9*, 2012, p. 244.

[4] Luo, A. A., Powell, B. R., Balogh, M. P.: Metall. Mater. Trans. A, *33*, 2002, p. 567. doi:10.1007/s11661-002-0118-1

[5] Nami, B., Razavi, H., Mirdamadi, S., Shabestari, S. G., Miresmaeili, S. M.: Metall. Mater. Trans. A, *41*, 2010, p. 1973. doi:10.1007/s11661-010-0238-y

[6] Baril, E., Labelle, P., Pekguleryuz, M.: JOM, *55*, 2003, p. 34. doi:10.1007/s11837-003-0207-7

[7] Carbonneau,Y., Couture, A., Van Neste, A.: Metall. Mater. Trans. A, *29*, 1998, p. 1759. doi:10.1007/s11661-998-0099-9

[8] Mazraeshahi, E. M., Nami, B., Miresmaeili, S. M., Tabatabaei, S. M.: Mater. Des., *76*, 2015, p. 64. doi:10.1016/j.matdes.2015.03.021

[9] Wang, H. Y., Jiang, Q. C., Ma, B. X., Wang, Y., Wang, J. G., Li, J. B.: J. Alloys Compd., *105*, 2005, p. 105. doi:10.1016/j.jallcom.2004.06.027

[10] Emley, E.: Principles of Magnesium Technology. New York, Pergamon Press 1966.

[11] Chu, S. N., Li, J. C. M.: J. Mater. Sci., *12*, 1977, p. 2200. doi:10.1007/BF00552241

[12] Kabirian, F., Mahmudi, R.: Metall. Mater. Trans. A, *40*, 2009, p. 116. doi:10.1007/s11661-008-9699-7

[13] Kondori, B., Mahmudi, R.: Metall. Mater. Trans. A, *40*, 2009, p. 2007. doi:10.1007/s11661-009-9867-4

[14] Rashno, S., Nami, B., Miresmaili, S. M.: Mater. Des., *60*, 2014, p. 289. doi:10.1016/j.matdes.2014.03.072

[15] Keyvani, M., Mahmudi, R., Nayyeri, G.: Metall. Mater. Trans. A, *42*, 2011, p. 1990. doi:10.1007/s11661-010-0564-0

[16] Slutsky, L. J., Garland, C. M.: Phys. Rev., *107*, 1957, p. 972. doi:10.1103/PhysRev.107.972

[17] Srinivasan, A., Swaminathan, J., Pillai, U. T. S., Guguloth, K., Pai, B. C.: Mater. Sci. Eng. A, *485*, 2008, p. 86. doi:10.1016/j.msea.2007.09.059

[18] Kassner, M. E., Prado, M. T. P.: Fundamentals of Creep in Metals and Alloys. New York, Elsevier 2004. doi:10.1016/b978-0-08-043637-1.x5000-5

[19] Nami, B., Razavi, H., Miresmaeili, S. M., Mirdamadi, Sh., Shabestari, S. G.: Scripta Mater., *65*, 2011, p. 221. doi:10.1016/j.scriptamat.2011.04.011

[20] Nami, B., Shabestari, S. G., Razavi, H., Mirdamadi, S., Miresmaeili, S. M.: Mater. Sci. Eng. A, *528*, 2011, p. 1261. doi:10.1016/j.msea.2010.10.004

[21] Somekawa, H., Hirai, K., Watanabe, H., Takigawa, Y., Higashi, K.: Mater. Sci. Eng. A, *407*, 2005, p. 53. doi:10.1016/j.msea.2005.06.059

[22] Zhu, S. M., Nie, J. F., Mordike, B. L.: Metall. Mater. Trans. A, *37*, 2006, p.1221. doi:10.1007/s11661-006-1073-z

[23] Chung, S. W., Watanabe, H., Kim, W. J., Higashi, K.: Mater. Trans., *45*, 2004, p. 1266. doi:10.2320/matertrans.45.1266

[24] Wang, W. Y., Shang, S. L., Wang, Y., Mei, Zh. G., Darling, K. A., Kecskes, L. J.: Mater. Res. Lett., *2*, 2013, p. 29. doi:10.1080/21663831.2013.858085